Journal of Power Sources 196 (2011) 9946–9954

Contents lists available at SciVerse ScienceDirect

Journal of Power Sources

journal homepage: www.elsevier.com/locate/jpowsour

Cross-linked miscible blend membranes of sulfonated poly(arylene ether sulfone) and sulfonated polyimide for polymer electrolyte fuel cell applications

Shouwen Chen[a,b], Xuan Zhang[a,b], Kangcheng Chen[b], Nobutaka Endo[b], Mitsuru Higa[b], Ken-ichi Okamoto[b,*], Lianjun Wang[a]

[a] School of Chemical Engineering, Nanjin University of Science and Technology, 200 Xiao Ling Wei, Nanjing 210094, China
[b] Graduate School of Science and Engineering, Yamaguchi University, Tokiwadai 2-16-1, Ube, Yamaguchi, 755-8611, Japan

ARTICLE INFO

Article history:
Received 22 April 2011
Received in revised form 16 July 2011
Accepted 22 August 2011
Available online 27 August 2011

Keywords:
Polymer electrolyte fuel cell
Cross-linked miscible blend membrane
Sulfonated poly(arylene ether sulfone)
Sulfonated polyimide
Membrane anisotropy

ABSTRACT

Cross-linked miscible blend (CMB) membranes were prepared from sulfonated poly(arylene ether sulfone) (SPAES) and sulfonated polynaphthalimide (SPI). They were transparent and insoluble in solvents. They showed the intermediate properties between SPAES and SPI concerning mechanical strength, water uptake, membrane swelling and proton conductivity. As for membrane swelling and proton conductivity, SPAES was almost isotropic, whereas SPI was highly anisotropic. CMB membranes were moderately anisotropic and had the advantages of the smaller *in-plane* membrane swelling and the larger *through-plane* conductivity compared to SPAES and SPI, respectively. Polymer electrolyte fuel cell performance of CMB2 membrane with an equal weight ratio of SPAES/SPI and an ion exchange capacity (IEC) of 1.74 meq g^{-1} was investigated, compared to SPI membrane (R1) with a slightly higher IEC of 1.86 meq g^{-1}. At 90 °C, 0.1 MPa and relatively high humidification of 82/68% RH or 0.2 MPa and low humidification of 50–30% RH, CMB2 showed the reasonably high cell performances. At 110 °C and 50–33% RH, the cell performance was fairly high only at a high pressure of 0.3 MPa, but low at 0.2–0.15 MPa. At these conditions, the cell performance was better for CMB2 than for R1 due to the more effective back-diffusion of water formed at cathode into membrane. CMB2 showed the fairly high PEFC durability at 110 °C.

1. Introduction

Polymer electrolyte fuel cells (PEFCs) have been attracting great attention as clean energy sources of residential cogeneration, vehicular transportation and other applications. Polymer electrolyte membrane (PEM) is a key component playing a critical role on PEFC performance. Perfluorosulfonic acid polymer membranes such as Nafion (DuPont) are state-of-the-art membranes because of their high proton conductivity and excellent chemical stability [1,2]. However, they have some disadvantages such as low operational temperatures below 80 °C and high fuel gas and oxygen crossover. Much research has been done to develop alternative PEMs based on sulfonated aromatic polymers [1,3–38].

Among alternative PEM materials, sulfonated poly(arylene ether)s (SPAEs) such as sulfonated poly(arylene ether sulfone)s (SPAESs) [7,8,12–23] and sulfonated poly(arylene ether ketone)s (SPAEKs) [24–26] are one of the promising candidates for fuel cell applications due to their good thermal and chemical stability. Proton conductivity and membrane stability are the most important properties determining the fuel cell applications. Generally, the proton conductivity significantly depends on the sulfonation level (or ion exchange capacity, IEC) and the water content sorbed in membrane. High proton conductivity can be achieved by controlling a relatively high sulfonation level (e.g. IEC > 2.0 meq g^{-1}). Unfortunately, for SPAEs, such a high IEC makes them excessively swell and even soluble in water. Cross-linking is a common method to suppress membrane swelling and to improve the membrane durability [4,39–42].

Sulfonated copolynaphthalimides (SPIs) are another type of promising candidates for fuel cell applications [27–38]. Recently we reported on side-chain-type SPIs derived from 1,4,5,8-naphthalene tetracarboxylic dianhydride (NTDA), 2,2′-bis(3-sulfophenoxy) benzidine (BSPOB) and a nonsulfonated diamine such as 1,3-bis(4-aminophenoxy)-benzene (BAPBz) [29,30] and their SO_2-crosslinked membranes [32–34]. They showed high performance and durability for PEFCs operated at 90 °C and in wide humidity range of 84–30% RH. These SPI membranes have anisotropic membrane properties. The membrane swelling is about ten times larger in thickness direction than in plane direction, whereas the proton conductivity is 40–50% larger in plane direction than in thickness direction. For PEFC applications, the smaller *in-plane* membrane swelling is suitable but the smaller *through-plane* proton conductivity is not. On the other hands, SPAEs are considered to have the

* Corresponding author. Tel.: +81 836 85 9203; fax: +81 836 85 9601.
E-mail addresses: okamotok@yamaguchi-u.ac.jp, okamotok@po.cc.yamaguchi-u.acv.jp (K.-i. Okamoto).

0378-7753/$ – see front matter © 2011 Elsevier B.V. All rights reserved.
doi:10.1016/j.jpowsour.2011.08.091

isotropic membrane properties. The large water uptake causes the large *in-plane* swelling and large *through-plane* conductivity, which are suitable and unsuitable, respectively, for PEFC applications.

Interpenetrating network or cross-linking of miscible blend is another powerful method to control and enhance the membrane properties. It is interesting to prepare cross-linked miscible blend (CMB) membranes of SPAE and SPI and to investigate their PEFC performance as well as anisotropy of membrane property.

In this paper we report on preparation of CMB membranes of SPAES and BSPOB-based SPI and on their properties including PEFC performance at higher temperatures of 90–110 °C and relative humidity of 82–30% RH.

2. Experimental

2.1. Materials

4,4′-Difluorodiphenyl sulfone (DFPS), sulfuric acid, sulfuric acid fuming (60%), 1-methyl-2-pyrrolidone (NMP), *m*-cresol, methanol, potassium carbonate and other reagents were purchased from Wako and used as received. Biphenol (BP) was purchased from Aldrich and purified by recrystallization from benzene and dried in vacuum at 100 °C for 24 h. 3,3′-Disulfonated-4,4′-difluorodiphenyl sulfone (SDFPS) was prepared by sulfonation of DFPS at 120 °C using fuming sulfonic acid (30% SO_3). Ultra-pure water was obtained from a Millipore Milli-Q purification system.

SPI with an equal molar ratio of BSPOB/BAPBz, NTDA-BSPOB/BAPBz(1/1), was prepared according to the literature [29].

SPAES with a molar ratio 3/2 of SDFPS/DFPS, BP-SDFPS/DFPS(3/2), was prepared as described below. To a dried 100 ml four necked flask equipped with N_2 inlet and outlet, 2.750 g (6 mmol) of SDFPS, 1.017 g (4 mmol) of DFPS, 1.862 g (10 mmol) of BP and 23 ml of NMP were charged. After the solids were completely dissolved, 2.070 g of K_2CO_3 was added. The reaction mixture was heated at 120 °C for 4 h and at 150 °C for another 20 h. After cooling to 60 °C, the mixture was diluted with 15 ml of NMP and poured into 300 ml of water. The fiber-like precipitate was collected by filtration, and washed with water several times.

2.2. Preparation of cross-linked miscible blend (CMB) membranes

SPAES (in potassium salt form) and SPI (in triethyl amine salt form) in a series of weight ratio (3/2, 1/1 and 2/3) were dissolved in *m*-cresol with a concentration of 7–10 wt%. After filtration, the filtrate was cast onto glass plates and the temperature was raised up to 120 °C and kept for 12 h. The as-cast membranes were soaked in methanol at 30 °C for 48 h and then proton-exchanged with 1.0 M hydrochloric acid at 50 °C for 72 h. The proton-exchanged membranes were thoroughly washed with water and then cured using stainless steel frames in vacuum at 150 °C for 1 h and then at 180 °C for 1 h. The SPAES/SPI blend membranes obtained were transparent and 35–45 μm in thickness.

The dry SPAES/SPI blend membranes in proton form were immersed into a solution of phosphorous pentoxide and methane sulfonic acid (1/10 in weight ratio; PPMA) at 40 °C for 30 h to form CMB membranes with SO_2-crosslinking [43,44]. The CMB membranes were thoroughly washed with water and then dried in vacuum at 150 °C for 2 h. The schematic structure of SPAES/SPI CMB membrane is shown in Fig. 1.

2.3. Membrane characterization

Mechanical tensile tests were performed on a universal testing machine (Orientic, TENSILON TRC-1150A) at 20 °C and 50% RH. Scanning electron microscopy (SEM) was performed using a JEOL JSM-6335F instrument. The cross sectional samples were prepared by cutting membrane sheets with a razor. Ion exchange capacity (IEC) was determined by a titration method. A sample membrane in proton form was soaked in a 15 wt% NaCl solution at 40 °C for 72 h to exchange the H^+ ion with Na^+ ion. Released protons were titrated by a 0.02 N NaOH solution using phenolphthalein as an indicator.

Water uptake was measured by soaking a sample sheet in water at 30 °C for 24 h. Then the membrane was taken out, wiped with tissue paper very quickly, and weighed on a microbalance. Water uptake (WU) was calculated from Eq. (1):

$$\mathrm{WU} = \frac{W_s - W_d}{W_d} \times 100\% \quad (1)$$

where W_d and W_s are the weights of dry and corresponding water-swollen membranes, respectively.

Dimensional changes in thickness (Δt) and in plane direction (Δl) were measured by soaking more than two sample sheets in water at 30 °C for 12 h and calculated from Eq. (2).

$$\Delta t = \frac{t - t_d}{t_d}$$
$$\Delta t = \frac{l - l_d}{l_d} \quad (2)$$

where t_d and l_d are the thickness and length of the dry membrane, respectively; t and l refer to those of the membrane swollen in water.

In-plane and *through-plane* proton conductivity ($\sigma_{\parallel}$ and $\sigma_{\perp}$, respectively) of SPI membrane was determined using an electrochemical impedance spectroscopy technique over the frequency from 10 Hz to 100 kHz (Hioki 3532-80). The cell was placed under either in a thermo-controlled humidic chamber or in liquid water [29]. For $\sigma_{\perp}$, a membrane sample was set between two platinum plate electrodes of 1 cm^2 area, and mounted on two Teflon blocks [30]. The cell was placed in liquid water. Proton conductivity ($\sigma_{\parallel}$ and $\sigma_{\perp}$) was calculated from Eq. (3):

$$\sigma_{\parallel} = \frac{d}{t_s w_s R}$$
$$\sigma_{\perp} = \frac{t_s}{AR} \quad (3)$$

where d is the distance between the two electrodes, t_s and w_s are the thickness and width of the membrane at a standard condition of 70% RH, respectively, A is the electrode area, and R is the resistance value measured. The thickness of a water-swollen membrane was used in the calculation of both $\sigma_{\parallel}$ and $\sigma_{\perp}$ in the fully hydrated state.

2.4. Fabrication of membrane electrode assembly (MEA) and measurements of cell performance

An MEA was fabricated from a membrane sample and Pt/C electrodes (Johnson Matthey Plc., #45372) by hot-pressing an electrode/membrane/electrode sandwich at 150 °C for 5 min under 60 kgf cm^{-2}. Prior to the hot-pressing, both surfaces of the membrane were impregnated with a small amount of Nafion solution as a binder. The effective electrode area was 5 cm^2. The MEA was set in a single cell test fixture and mounted in to an in-house fuel cell test station (NF Inc., model As-510), which was supplied with temperature-controlled humidified gases.

The PEFC performance was evaluated at cell temperatures of 90–110 °C and back pressures of 0.3–0.1 MPa and different gas humidification temperatures of 91–61 °C. The gas flow was controlled to keep constant utilization of H_2/air at 60/15%, 70/32% and 80/50–60% under anode/cathode gas humidification conditions of 82/68, 50/50 and 30/30 (33/33) %RH, respectively. The cell resistance (R_c) and electrode reaction resistance (R_{el}) were determined by the AC impedance cole–cole plots. The *through-plane* proton conductivity under PEFC operation ($\sigma_{\perp,FC}$) was evaluated by assuming

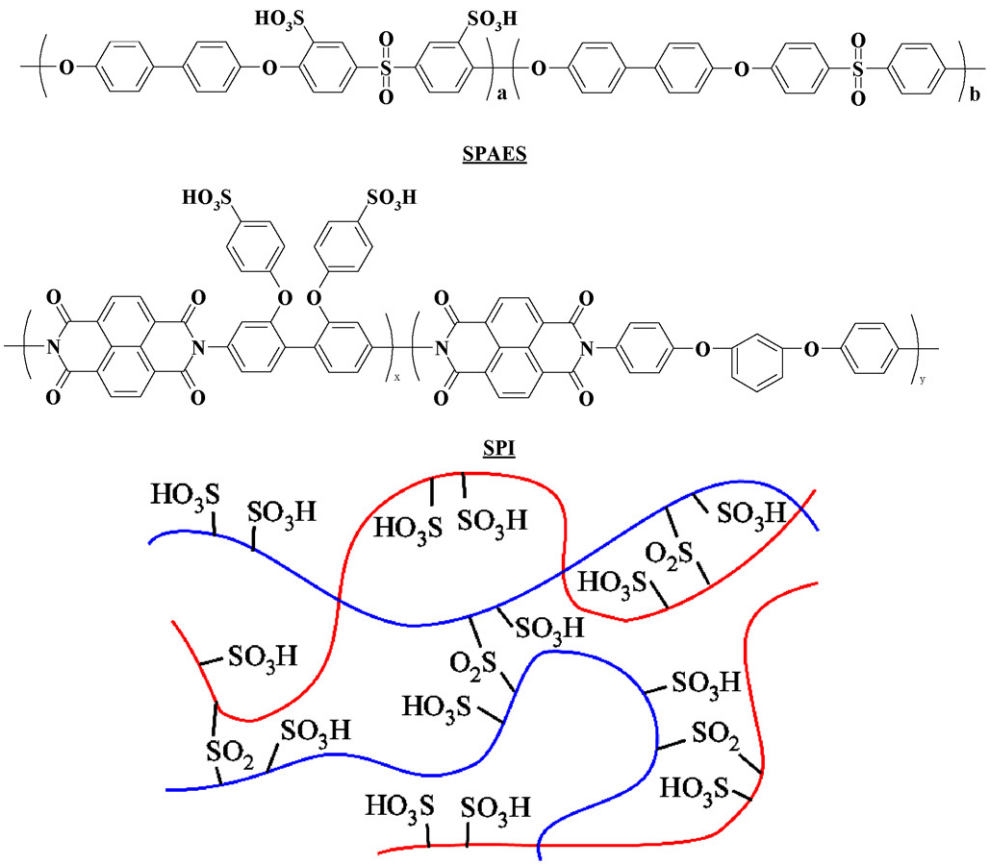

Fig. 1. Schematic chemical structure of SPAES/SPI CMB membrane.

that the membrane resistance is approximately equal to the cell resistance.

Hydrogen crossover across a membrane was measured by linear sweep voltammetry at a cell temperature of 90 °C, an anode/cathode gas humidification temperature of 85/85 °C (82% RH) and a back pressure of 0.2 MPa. The potential of the cathode (in N_2) was swept at 0.5 mV s^{-1} from 50 mV to 500 mV vs. reference. Hydrogen crossover was evaluated as the diffusion-limited hydrogen oxidation current obtained in the range of 300–400 mV vs. reference.

3. Results and discussion

3.1. Physicochemical properties

In this study, BP-SDFPS/DFPS(3/2) with a high IEC of 2.40 meq g^{-1} and NTDA-BSPOB/BAPBz(1/1) with a low IEC of 1.56 meq g^{-1} were used as SPAES and SPI, respectively. They had high reduced viscosities of 1.2 dL g^{-1} in DMSO solution (1% LiCl) and 5.6 dL g^{-1} in *m*-cresol, respectively, at 35 °C and 0.5 g dL^{-1}. The blend membranes of SPAES/SPI with weight ratios of 3/2, 1/1 and 2/3 (Blends 1, 2 and 3, respectively) were prepared by solution cast method and were transparent. They were subjected to the cross-linking treatment with PPMA, where the cross-linking via sulfonyl ($-SO_2-$) bond was formed by the chemical reaction between the sulfonic acid groups and the activated (electron rich) phenyl rings in the BAPBz and BP moieties as shown in Scheme 1 [43,44]. After the treatment the blend membranes were insoluble in *m*-cresol containing triethyl amine, although being soluble before, indicating the formation of cross-linking.

Table 1 lists the physicochemical properties of SPAES, SPI, blend and CMB membranes together with those of NTDA-BSPOB/BAPBZ(2/1) (R1) and Nafion 112 membranes cited for comparison. The SO_2-crosslinked (40 °C, 30 h) membrane of R1 (R1X) was also cited. The experimental IEC values determined by titration method for the blend membranes were slightly (4–5%) lower than the theoretical ones calculated from the feed ratios, which was often observed for SPI membranes. The CMB membranes showed the lower experimental IEC values (by 5% for CMB1 and 7% for CMB2 and CMB3) than the corresponding blend membranes, indicating the consumption of small amounts (5–7%) of sulfonic

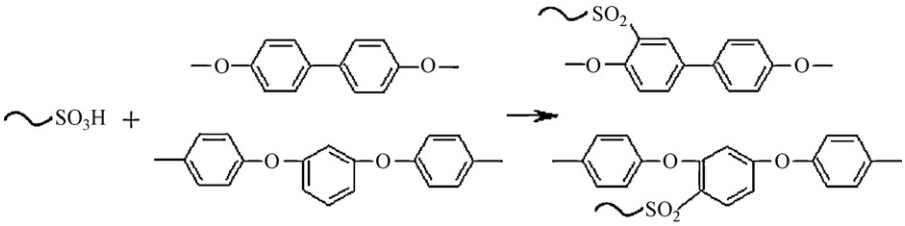

Scheme 1. Formation of cross-linking via sulfonyl bond.

Table 1
Physicochemical properties of SPAES, SPI, Blend, CMB and Nafion 112 membranes.

Code	Polymer	IEC[a] (meq g^{-1})	WU[b] (%)	λ	Size change[b]		$\Delta t/\Delta l$	$\sigma_{\parallel}$ [c]			$\sigma_{\perp}$ [d]	$\sigma_{\perp}/\sigma_{\parallel}$
					Δt (%)	Δl (%)		50 (mS cm^{-1})	70 (mS cm^{-1})	Water (mS cm^{-1})	Water (mS cm^{-1})	
SPAES	x/y = 3/2	2.40 (2.35)	123	29	34	27	1.3	11	43	261	245	0.94
SPI	x/y = 1/1	1.56 (1.51)	52	19	35	3.6	9.7	4.6	23	85	56	0.66
Blend1	SPAES/SPI(3/2)	2.06 (1.96)	90	26	36	16	2.3	8.3	34	176		
CMB1	SPAES/SPI(3/2)-XSO_2	(1.87)	71	21	33	14	2.4	7.6	30	154	126	0.82
Blend2	SPAES/SPI(1/1)	1.98 (1.87)	75	22	33	13	2.5	7.8	27	161		
CMB2	SPAES/SPI(1/1)-XSO_2	(1.74)	59	19	29	12	2.4	7.5	26	146	121	0.83
Blend3	SPAES/SPI(2/3)	1.90 (1.82)	72	22	32	14	2.3	7.3	37	147		
CMB3	SPAES/SPI(2/3)-XSO_2	(1.69)	63	21	30	12	2.4	6.5	34	133	106	0.79
R1	SPI(x/y = 2/1)	1.96 (1.86)	76	23	47	3.9	12	8.6	33	165	116	0.70
R1X	SPI(x/y = 2/1)-XSO_2	(1.73)	72	23	43	5.0	8.6	6.1	27	148	107	0.72
Nafion 112		0.91(0.89)	39	24	16	14	1.1	26	54	139	136	0.98

[a] Calculated vales; data in parentheses are the values measured by titration method.
[b] At 30 °C.
[c] At 50% RH, 70% RH and in water at 60 °C.
[d] In water at 60 °C.

acid group by the cross-linking reaction. This was similar to the case of R1X.

The blend and CMB membranes were not opaque but transparent, indicating the homogeneous mixing of SPAES and SPI in optical level. In SEM observation, as shown in Fig. 2, the membranes showed the absence of inhomogeneity of blend in μm to 100 nm scale. From these results, we considered that the miscible blend and CMB membranes were prepared in this study.

The thermal stability evaluated by TGA was similar among the blend and CMB membranes. The first decomposition (desulfonation) temperature was about 300 °C, which was comparable to those of SPAES and SPI.

Fig. 3 shows the tensile stress-strain curves of SPAES, SPI, Blend2 and CMB2 membranes. The mechanical property was characterized by Young's modulus (M), maximum stress (S) and elongation at break (E). The data are also listed in Fig. 3. The M, yield point and S were about two times larger for SPI than for SPAES, whereas the E was 2.7 times larger for SPAES. The CMB2 showed the intermediate mechanical property between SPAES and SPI, which was slightly better than that of Blend2.

The water uptake (WU) mainly depends on the IEC of membrane, and comparison of them is often performed in terms of the number of water molecules sorbed per sulfonic acid group, λ. Generally, the λ still depends on IEC and is slightly larger for the higher IEC. The λ values listed in Table 1 were calculated using the experimental IEC values. SPAES showed the larger λ value of 29 than SPI (λ = 19). Blend1 with the higher SPAES content showed the higher λ value of 26, being close to that of SPAES, whereas Blend2 and Blend3 showed the intermediate λ value of 22. The CMB membranes showed the lower λ values of 19–21 than the blend membranes.

The *through-plane* and *in-plane* dimensional change (Δt and Δl, respectively) and the anisotropic membrane swelling ratio ($\Delta t/\Delta l$) are summarized in Table 1. The membrane swelling was almost isotropic for SPAES, but significantly anisotropic for SPI ($\Delta t/\Delta l$ = 10). In the blend and CMB membranes, the alignment of SPI molecules in plane direction was disturbed by SPAES molecules and as a result the anisotropy in membrane swelling was weakened. The blend and CMB membranes had the intermediate $\Delta t/\Delta l$ values of 2.3–2.5. It is noted that CMB2 and CMB3 had the larger

Table 2
PEFC performances of CMB2, SPI (R1) and Nafion 112 membranes.

Conditions[a]	Code	OCV (V)	$V_{0.5}$ (V)	W_{max} (W cm^{-2})	$\sigma_{\perp,FC}$ [b] (mS cm^{-1})	R_{el} [b] (mΩ cm^2)
90/0.2/82	CMB2	0.96	0.69	>0.90	49	113
	R1	0.97	0.70	>0.88	38	130
	Nafion 112	0.93	0.69	>0.86	90	197
90/0.1/82	CMB2	0.95	0.61	0.59	37	194
	R1	0.96	0.62	0.54	28	211
90/0.2/50	CMB2	0.97	0.67	0.75	38	167
	R1	0.99	0.69	0.67	31	240
	Nafion 112	0.94	0.68	0.75	70	263
90/0.15/50	CMB2	0.97	0.57	0.40	19	212
90/0.1/50	CMB2	0.96	0.49	0.28	13	311
90/0.2/30	CMB2	0.98	0.66	0.58	33	310
	R1	1.00	0.65	0.50	23	279
	Nafion 112	0.93	0.66	0.57	58	486
90/0.15/30	CMB2	0.98	0.48	0.24	(11)	–
	R1	0.98	0.42	0.21	(7)	–
110/0.3/50	CMB2	0.98	0.67	0.66	36	–
	R1	0.98	0.51	0.47	27	–
110/0.2/50	CMB2	0.98	0.57	0.35	(18)	(270)
	R1	0.98	0.51	0.28	(13)	–
110/0.3/33	CMB2	0.98	0.61	0.37	(17)	(189)
	R1	1.00	0.51	0.26	(10)	–
110/0.2/33	CMB2	0.97	(0.43)[c]	0.13	(4)[c]	–

[a] PEFC operation conditions ($x/y/z$); x, y and z refer to cell temperature (°C), gas pressure (MPa) and gas relative humidity (%RH), respectively.
[b] At 1 A cm^{-2}; the data in parenthesis were measured at 0.5 A cm^{-2}.
[c] At 0.35 A cm^{-2}.

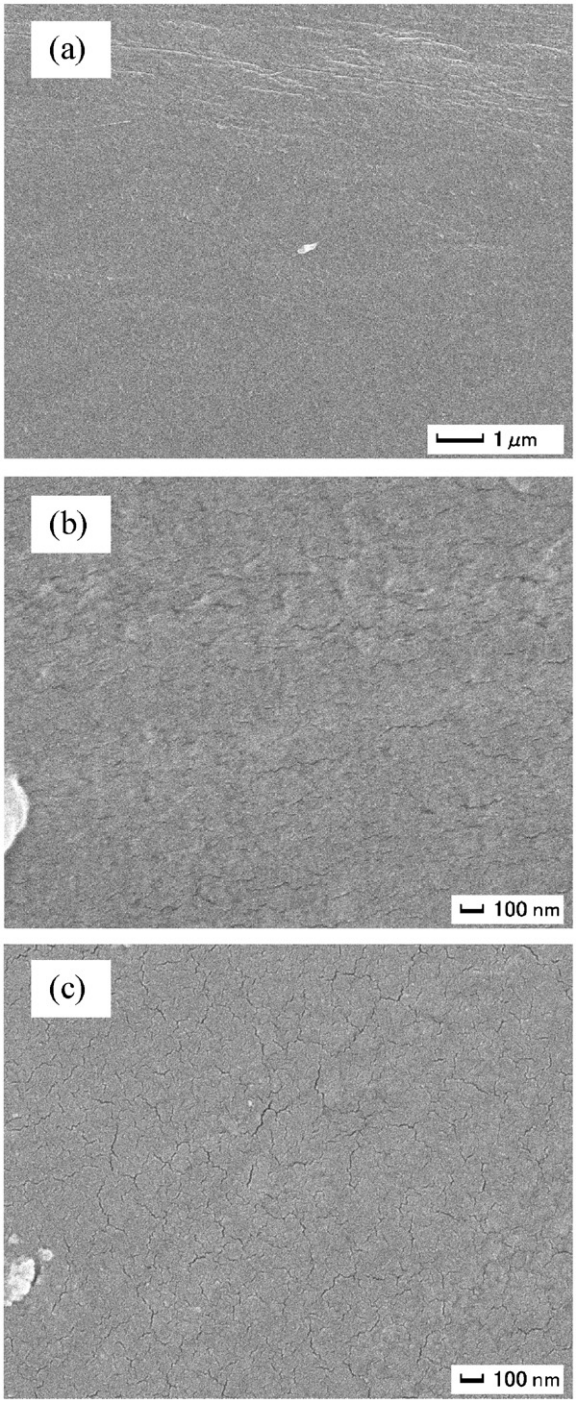

Fig. 2. SEM images of CMB2 membrane. (a) Cross section, × 10000; (b) cross section, × 50000 (c) surface, × 50000.

water uptakes (about 60%) than Nafion 112 but the rather smaller *in-plane* dimensional change (12%).

3.2. Proton conductivity

The *in-plane* proton conductivity ($\sigma_{\parallel}$) at 60 °C as a function of relative humidity (RH) is summarized in Table 1. The conductivity largely depends on IEC and water uptake. The $\sigma_{\parallel}$ of CMB membranes was slightly smaller than that of the blend membranes, and was in the order of CMB1 > CMB2 > CMB3. As shown in Fig. 4, the relative humidity dependence of $\sigma_{\parallel}$ for the blend and CMB

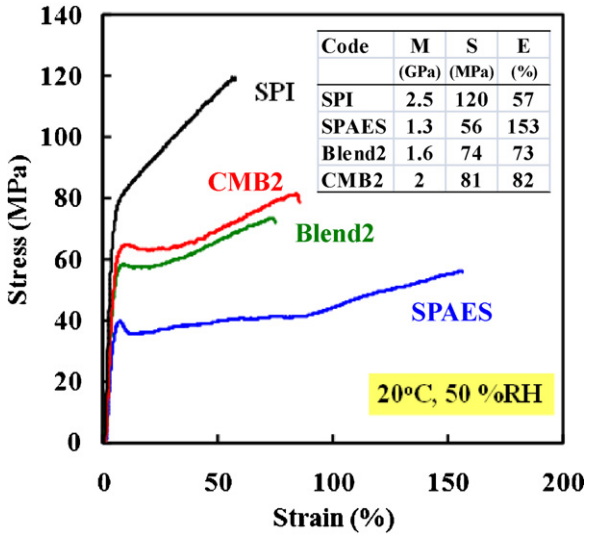

Fig. 3. Tensile stress–strain curves of SPAES, SPI, Blend2 and CMB2 membranes.

membranes was similar to that of SPAES and SPI, and was much larger than that for Nafion 112. Compared with Nafion 112, the CMB membranes showed the larger or comparable *in-plane* conductivities in water but 3.5–4 times smaller conductivities at 50% RH.

The *through-plane* conductivity ($\sigma_{\perp}$) in water at 60 °C and the anisotropic proton conductivity ratio ($\sigma_{\perp}/\sigma_{\parallel}$) are summarized in Table 1. The proton conductivity was almost isotropic for SPAES ($\sigma_{\perp}/\sigma_{\parallel}$ = 0.94), but considerably anisotropic for SPI ($\sigma_{\perp}/\sigma_{\parallel}$ = 0.66). The CMB membranes showed the moderately anisotropic conductivity with $\sigma_{\perp}/\sigma_{\parallel}$ values of 0.79–0.83. The $\sigma_{\perp}$ was in the order of CMB1 > CMB2 > CMB3. Among the CMB membranes, CMB2 seemed as best for PEFC application from consideration of water uptake, *in-plane* membrane swelling and *through-plane* proton conductivity. It is noted that CMB2 had the larger $\sigma_{\perp}$ (121 mS cm^{-1}) than R1X and R1 (107 and 116 mS cm^{-1}, respectively) in spite of the similar or slightly lower IEC due to the smaller conductivity anisotropy.

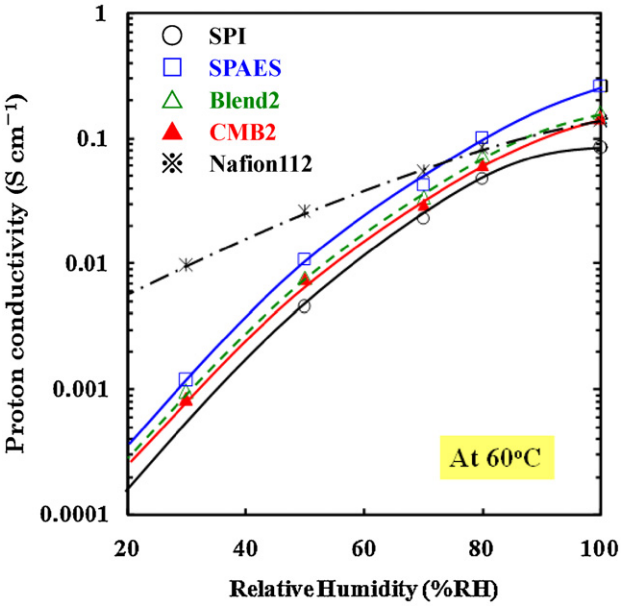

Fig. 4. Relative humidity dependence of proton conductivity ($\sigma_{\parallel}$) of SPAES, SPI, Blend2, CMB2 and Nafion 112 membranes at 60 °C.

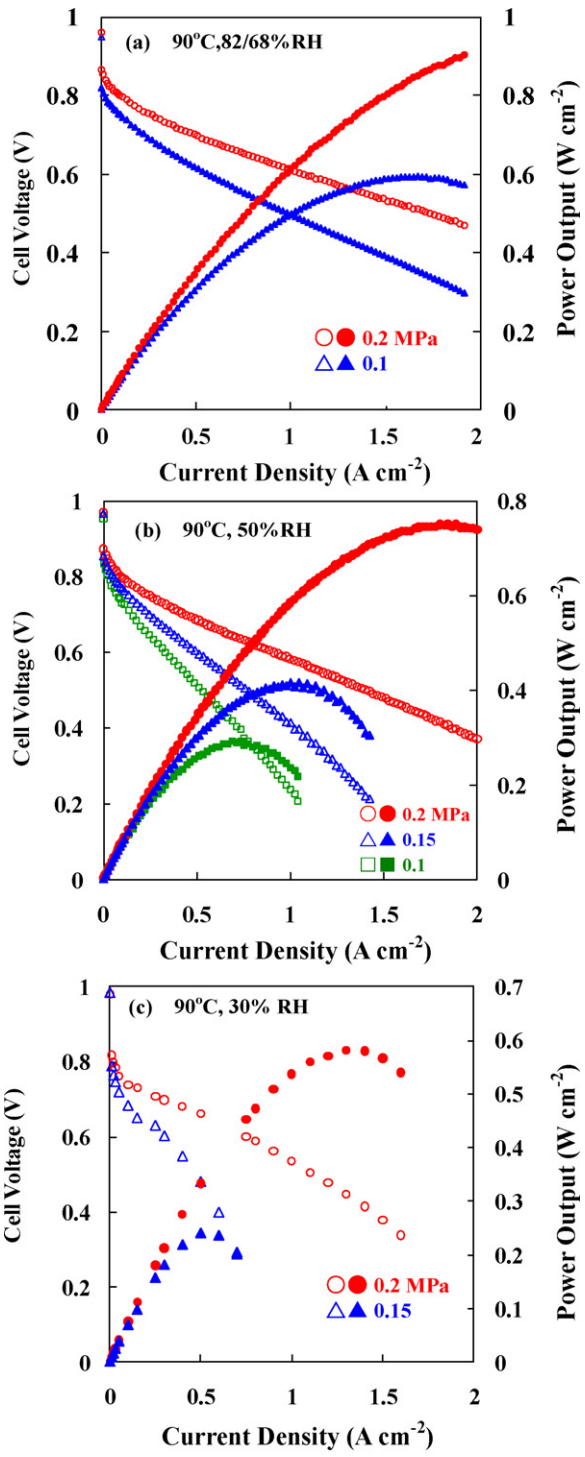

Fig. 5. PEFC performances of CMB2 at 90 °C, gas pressures of 0.2–0.1 MPa and gas humidification of (a) 82/68% RH, (b) 50% RH and (c) 30% RH.

3.3. PEFC performance

Fig. 5(a)–(c) shows the effects of pressure and gas humidity on PEFC performance for CMB2 at a cell temperature of 90 °C. Anode/cathode gas humidification temperatures were set at 85/80, 72.8/72.8 and 61.3/61.3 °C, which corresponded to 82/68%, 50/50% and 30/30% RH, respectively (here after abbreviated to 82/68% RH, 50% RH and 30% RH). The CMB2 membranes used were 38 μm in thickness. Table 2 lists the PEFC performance data of open-circuit voltage (OCV), cell voltage at 0.5 A cm^{-2} ($V_{0.5}$), maximum output (W_{max}), the *through-plane* proton conductivity ($\sigma_{\perp,FC}$) and electrode reaction resistance (R_{el}). At 0.2 MPa and 82/68% RH, CMB2 showed the high cell performance, namely, $V_{0.5}$ of 0.69 V and W_{max} of above 0.90 W cm^{-2}. At 0.2 MPa, with decreasing the humidity from 82/68% RH to 50% RH and then to 30% RH, the cell performance decreased fairly (see the circle keys in Fig. 5(a)–(c)), but was still kept in a relatively high level even at 30% RH, namely, $V_{0.5}$ of 0.66 V and W_{max} of 0.58 W cm^{-2}. With decreasing the pressure from 0.2 to 0.1 MPa, the cell performance also decreased. The decreasing rate was larger at the lower humidification. At the relatively high humidification of 82/68% RH, the cell performance was still in a relatively high level, namely, $V_{0.5}$ of 0.61 V and W_{max} of 0.59 W cm^{-2} at ambient pressure. On the other hand, at the low humidification of 30% RH, the cell performance was in a low level, namely, $V_{0.5}$ of 0.48 V and W_{max} of 0.24 W cm^{-2} even at 0.15 MPa.

It is noted that the *through-plane* proton conductivity ($\sigma_{\perp,FC}$) under PEFC operation listed in Table 2 reflects the behavior of the cell performance mentioned above. At 82/68% RH, the $\sigma_{\perp,FC}$ values for CMB2 were 49 and 37 mS cm^{-1} at 0.2 and 0.1 MPa, respectively. At 0.2 MPa, the $\sigma_{\perp,FC}$ values were 38 and 33 mS cm^{-1} at 50% and 30% RH, respectively. These relatively large $\sigma_{\perp,FC}$ values were responsible for the relatively high cell performance at 0.2 MPa and the low humidification of 50% RH to 30% RH. On the other hand, the $\sigma_{\perp,FC}$ values were much smaller at the lower pressure and lower humidification, namely, 13 mS cm^{-1} at 0.1 MPa and 50% RH and 11 mS cm^{-1} at 0.15 MPa and 30% RH, which was responsible for the low cell performance at the corresponding conditions. This difference was due to the effectiveness of the back-diffusion of water formed at the cathode into membrane under PEFC operation. In general, the actual water content in membrane under PEFC operation is higher than that in membrane being in equilibrium with the water vapor in feed gas due to the back-diffusion of water, which is more effective at the higher pressure and lower humidification and for thinner membrane [33,34].

Fig. 6(a) and (b) shows the effects of pressure and gas humidity on PEFC performance for CMB2 at 110 °C. Anode/cathode gas humidification temperatures were set at 90.6 and 80.0 °C, which corresponded to 50%, and 33% RH, respectively. The PEFC performance data are also listed in Table 2. The cell performance at 110 °C and 50–33% RH was fairly high only at a high pressure of 0.3 MPa. At 0.2–0.15 MPa, it was much lower than that at 90 °C shown in Fig. 5(b) and (c). For example, at 110 °C, 0.2 MPa and 50% RH, the $V_{0.5}$ and W_{max} values were 0.57 V and 0.35 W cm^{-2}, respectively, which were 15% and 53% smaller than those at 90 °C. At the low humidification of 33% RH, the cell voltage significantly decreased with increasing load current density even at 0.2 MPa, resulting in a very low W_{max} of 0.13 W cm^{-2}, as shown in Fig. 6(b). These results were due to the much smaller $\sigma_{\perp,FC}$ values (18 and 4 mS cm^{-1} at 50% and 33% RH, respectively) at 0.2 MPa and 110 °C, indicating that the back-diffusion of produced water was much less effective at 110 °C than at 90 °C.

It is interesting to compare the PEFC performance between CMB2 and SPI membranes. R1X, SO_2-crosslinked SPI membrane with almost the same measured IEC value as that of CMB2, showed the worse PEFC performance than R1, the precursor membrane with the slightly higher IEC [33,34]. Therefore, R1 was chosen as SPI membrane for comparison. The results for R1 membranes (34 μm in thickness) cited from Ref. [34] are summarized in Table 2 and Fig. 7(a) and (b). At 90 °C and 82/68% RH, the cell performance at 0.2 MPa was high and almost the same for CMB2 and R1. On the other hand, at 0.1 MPa, it was slightly better for CMB2 than for R1 in the range of the higher load current density, resulting in the slightly larger W_{max} for CMB2 (0.59 W cm^{-2}) than for R1 (0.54 W cm^{-2}). At the lower humidification of 50% and 30% RH, the difference in the cell performance between CMB2 and R1 became larger, as shown in Fig. 7(a). For example, at 30% RH, 0.2 MPa and 90 °C, the W_{max} values

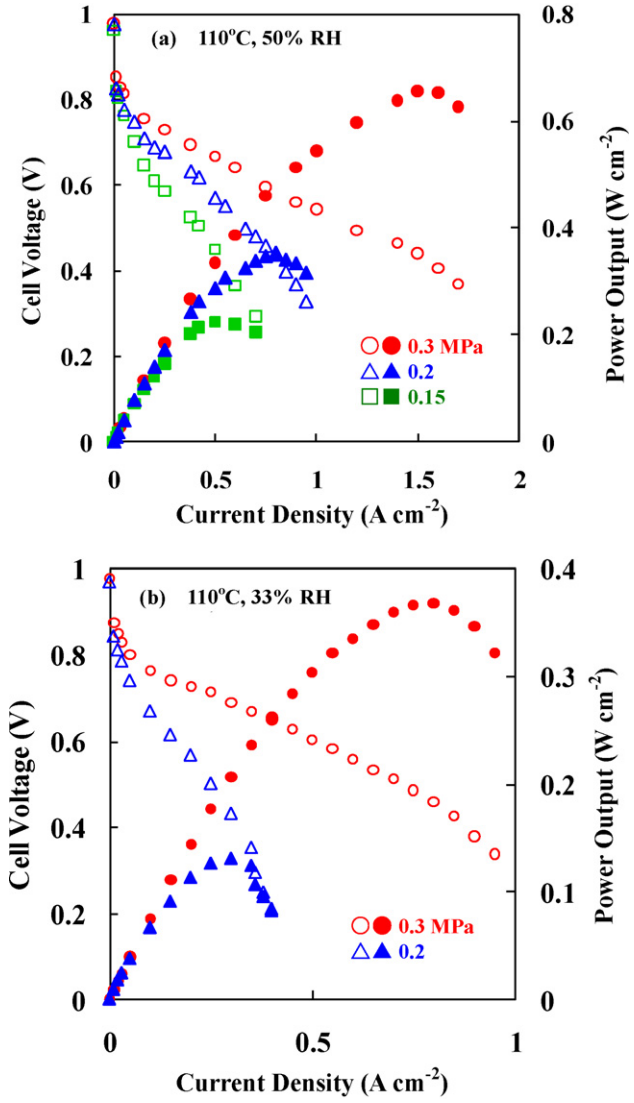

Fig. 6. PEFC performances of CMB2 at 110 °C, gas pressures of 0.3–0.15 MPa and gas humidification of (a) 50% RH and (b) 33% RH.

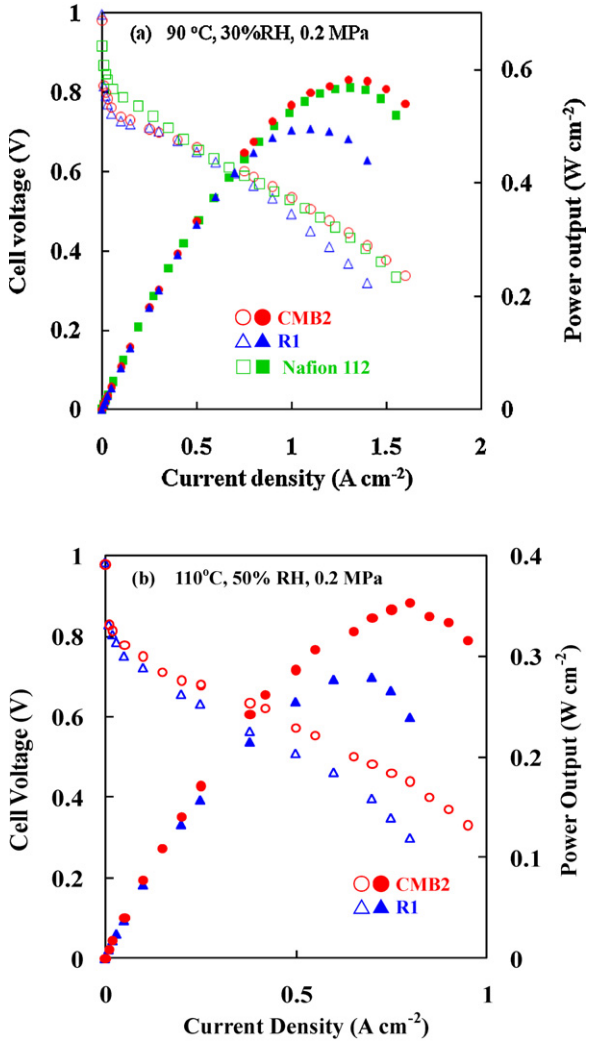

Fig. 7. PEFC performances of CMB2, R1 and Nafion 112 (a) at 90 °C, 30% RH and 0.2 MPa and (b) at 110 °C, 50% RH and 0.2 MPa.

were 0.58 and 0.50 W cm^{-2} for CMB2 and R1, respectively. The better cell performance for CMB2 was due to the larger $\sigma_{\perp,FC}$ value (33 mS cm^{-1}) than that for R1 (23 mS cm^{-1}). The similar results were also observed at 110 °C, as shown in Fig. 6(b). These facts indicated that the back-diffusion of water was more effective for CMB2 than for R1 probably due to the less anisotropic membrane morphology for the former.

The PEFC performance data at 90 °C for Nafion 112 cited from Ref. [34] are also listed in Table 2 and shown in Fig. 7(a). Nafion 112 showed the lower OCV values (0.93–0.94 V) and the larger $\sigma_{\perp,FC}$ values (90–58 mS cm^{-1}) than those for CMB2 (0.96–0.98 V and 49–33 mS cm^{-1}, respectively). Nafion 112 showed the high cell performance comparable to that for CMB2.

Hydrogen permeability coefficient (P_{H_2}) values were calculated from hydrogen crossover currents. The P_{H_2} data are presented in Barrer unit, namely, 1 Barrer = 1×10^{-10} cm^3 (STP) cm^{-3} s^{-1} cmHg^{-1}. The P_{H_2} value for Nafion 112 obtained in this study at 90 °C, 0.2 MPa and 82% RH was 113 Barrer, which was reasonable compared to the reported values at different measurement conditions [45,46]. The P_{H_2} values were 38, 29 and 24 Barrer for CMB2, R1 and R1X, respectively. CMB2 showed the slightly larger hydrogen permeability. This suggests the larger water-vapor permeability through CMB2 membrane, which is favorable to the back-diffusion of water.

The short-term durability test was carried out for a PEFC with CMB2 at 110 °C to check the mechanical and electrochemical

Table 3
PEFC performances of CMB2 before and after the durability test at 110 °C and 50–33% RH for a total of 300 h.

Conditions[a]	Durability test	OCV (V)	$V_{0.5}$ (V)	W_{max} (W cm^{-2})	$\sigma_{\perp,FC}$ [b] (mS cm^{-1})	R_{el} [b] (mΩ cm^2)
90/0.2/82	Before	0.96	0.69	>0.90	49	130
	After	0.86	0.66	>0.83	47	126
110/0.3/50	Before	0.98	0.67	0.66	38	190
	After	0.84	0.63	0.60	37	180

[a] PEFC performance measurement conditions (see Table 2).
[b] At 1 A cm^{-2}.

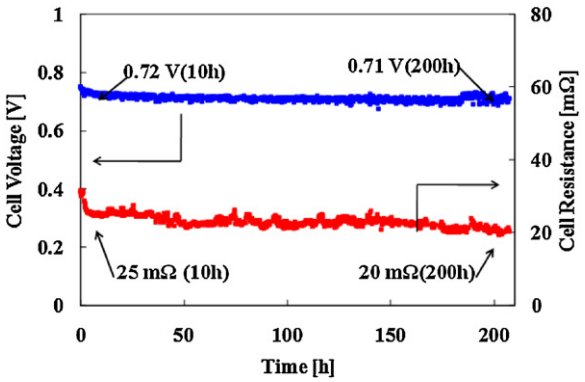

Fig. 8. Durability test for a PEFC with CMB2 operated under a constant load current density of 0.2 A cm^{-2} at 110 °C, 50% RH and 0.3 MPa.

durability of membrane. The cell was first operated under the different conditions (0.2–0.1 MPa, 82–30% RH and 0–1.9 A cm^{-2}) at 90 °C for 100 h, and then at 110 °C, 0.3–0.15 MPa and 50–33% RH for 90 h to measure polarization and power output curves. After these measurements, the cell was operated under a constant load current density of 0.2 A cm^{-2} at 110 °C, 50% RH and 0.3 MPa for 210 h with monitoring the cell voltage and resistance. As shown in Fig. 8 the cell voltage hardly decreased and the cell resistance slightly decreased. Before and after the durability test for a total of 300 h at 110 °C, the polarization and power output curves were measured at 90 °C, 82% RH and 0.2 MPa and also at 110 °C, 50% RH and 0.3 MPa. The results are shown in Fig. 9(a) and (b) and Table 3. The cell performance became slightly lower after the durability test. For example, at 110 °C, $V_{0.5}$ and W_{max} slightly decreased from 0.67 to 0.63 V and from 0.66 to 0.60 W cm^{-2}, respectively, whereas $\sigma_{\perp,FC}$ hardly changed (38–37 mS cm^{-1}). On the other hand, the OCV fairly decreased from 0.98 to 0.84 V. We reported the similar durability results at 110 °C for SO_2-crosslinked SPI (NTDA-BSPOB/BAPBz(3/1)) membranes with a measured IEC of 1.95 meq g^{-1} [34]. The results mentioned above indicated that CMB2 had the high PEFC durability at 110 °C comparable to that of the SO_2-crosslinked SPI membranes. The OCV drop at high temperature of 110 °C might be related with some degradation of the platinum catalyst [33,34,47].

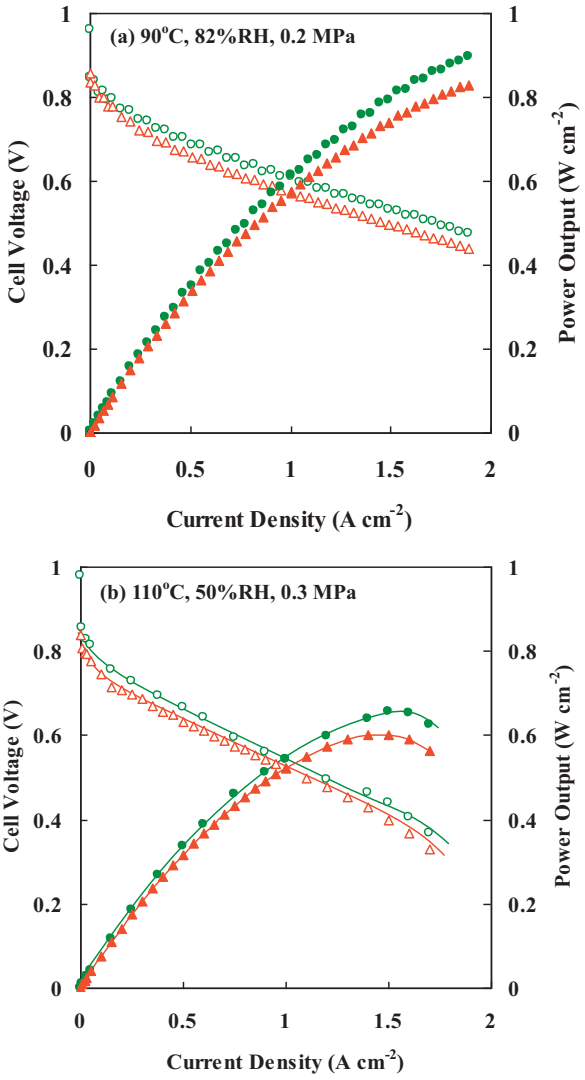

Fig. 9. PEFC performances of CMB2 before (○, ●) and after (△, ▲) the durability test at 110 °C, 50–33% RH and 0.3–0.15 MPa for a total of 300 h. PEFC measurement conditions are (a) 90 °C, 82% RH and 0.2 MPa and (b) 110 °C, 50% RH and 0.3 MPa.

4. Conclusions

CMB membranes of SPAES and SPI were insoluble in solvents, transparent, tough and ductile. They showed the intermediate properties between SPAES and SPI concerning mechanical strength, water uptake, membrane swelling and proton conductivity. SPAES showed almost the isotropic swelling and conductivity ($\Delta t/\Delta l = 1.3$ and $\sigma_\perp/\sigma_\parallel = 0.94$), whereas SPI showed the significantly anisotropic ones ($\Delta t/\Delta l = 10$ and $\sigma_\perp/\sigma_\parallel = 0.66$–$0.70$). The CMB membranes showed the moderately anisotropic swelling and conductivity ($\Delta t/\Delta l = 2.4$ and $\sigma_\perp/\sigma_\parallel = 0.79$–$0.83$) and had the advantages of the smaller *in-plane* membrane swelling compared to SPAES and the larger *through-plane* proton conductivity compared to SPI. CMB2 had the larger $\sigma_\perp$ than R1X and R1 in spite of the similar or slightly lower IEC.

At 90 °C, 0.2 MPa and relatively high humidification of 82/68% RH, CMB2 showed the high cell performance; $V_{0.5}$ of 0.69 V and W_{max} of above 0.90 W cm^{-2}. Either at 0.1 MPa and 82/68% RH or at 0.2 MPa and low humidification of 50–30% RH, the cell performance was still kept in a reasonably high level (for example, $V_{0.5}$ of 0.66 V and W_{max} of 0.58 W cm^{-2} at 0.2 MPa and 30% RH), but fairly low at 0.15–0.1 MPa and 50–30% RH. At 110 °C and 50–33% RH, the cell performance was much lower than that at 90 °C. The $\sigma_{\perp,FC}$ under PEFC operation reflected the behavior of the cell performance mentioned above; namely the larger $\sigma_{\perp,FC}$ was responsible for the better cell performance. CMB2 showed the better cell performance than R1, which was due to the more effective back-diffusion of water formed at cathode into membrane probably because of the less anisotropic membrane morphology. CMB2 showed the fairly high PEFC durability at 110 °C and 50–33% RH. The CMB membranes have potential for PEFC applications.

References

[1] O. Savadogo, J. New Mater. Electrochem. Syst. 1 (1998) 47–66.
[2] K.A. Mauritz, R.B. Moore, Chem. Rev. 104 (2004) 4535–4586.
[3] M. Rikukawa, K. Sanui, Prog. Polym. Sci. 25 (2000) 1463–1502.
[4] J.A. Kerres, J. Membr. Sci. 185 (2001) 3–27.
[5] K.D. Kreuer, J. Membr. Sci. 185 (2001) 29–39.
[6] Q. Li, R. He, J.O. Jensen, N. Bjerrum, Chem. Mater. 15 (2003) 4896–4915.
[7] M.A. Hickner, H. Ghassemi, Y.S. Kim, B.R. Einsla, J.E. McGrath, Chem. Rev. 145 (2004) 4587–4612.
[8] W.L. Harrison, M.A. Hickner, Y.S. Kim, J.E. McGrath, Fuel Cells 5 (2005) 201–212.
[9] Y. Yin, O. Yamada, K. Tanaka, K. Okamoto, Polym. J. 38 (2006) 197–219.
[10] C. Marestin, G. Gebel, O. Diat, R. Mercier, Adv. Polym. Sci. 216 (2008) 185–258.
[11] K. Goto, I. Rozhanskii, Y. Yamakawa, T. Otsuki, Y. Naito, Polym. J. 41 (2009) 95–105.
[12] H. Ghassemi, J.E. McGrath, T.A. Zawodzinski Jr., Polymer 47 (2006) 4132–4139.

[13] Y. Li, A. Roy, A.S. Badami, M. Hill, J. Yang, S. Dunn, J.E. McGrath, J. Power Sources 172 (2007) 30–38.
[14] H. Lee, A. Roy, O. Lane, M. Lee, J.E. McGrath, J. Polym. Sci. A: Polym. Chem. 48 (2010) 214–222.
[15] H.S. Lee, A. Badami, A. Roy, J.E. McGrath, J. Polym. Sci. A: Polym. Chem. 45 (2007) 4879–4890.
[16] M.L. Einsla, Y.S. Kim, M. Hawley, H.S. Lee, J.E. McGrath, B. Liu, M.D. Guiver, B.S. Pivovar, Chem. Mater. 20 (2008) 5636–5642.
[17] K. Miyatake, Y. Chikashige, E. Higuchi, M. Watanabe, J. Am. Chem. Soc. 129 (2007) 3879–3887.
[18] B. Bae, T. Yoda, K. Miyatake, H. Uchida, M. Watanabe, Angew. Chem. Int. Ed. 49 (2010) 317–320.
[19] T. Yamaguchi, H. Zhou, S. Nakazawa, N. Hara, Adv. Mater. 19 (2007) 592–596.
[20] K. Nakabayashi, K. Matsumoto, M. Ueda, J. Polym. Sci. A: Polym. Chem. 46 (2008) 3947–3957.
[21] K. Matsumoto, T. Higashihara, M. Ueda, Macromolecules 42 (2009) 1161–1166.
[22] D.S. Kim, G.P. Robertson, M.D. Guiver, Macromolecules 41 (2008) 2126–2134.
[23] D.S. Kim, G.P. Robertson, Y.S. Kim, M.D. Guiver, Macromolecules 42 (2009) 957–963.
[24] P.X. Xing, G.P. Robertson, M.D. Guiver, S.D. Mikhailenko, S. Kaliaguine, Macromolecules 37 (2004) 7960–7967.
[25] X.F. Li, C.J. Zhao, H. Lu, Z. Wang, H. Na, Polymer 46 (2005) 5820–5827.
[26] B. Liu, G. Robertson, D.S. Kim, M.D. Guiver, W. Hu, Z. Jiang, Macromolecules 40 (2007) 1934–1944.
[27] X. Guo, J. Fang, T. Watari, K. Tanaka, H. Kita, K. Okamoto, Macromolecules 35 (2002) 6707–6713.
[28] Y. Yin, O. Yamada, S. Hayashi, K. Tanaka, H. Kita, K. Okamoto, J. Polym. Sci. Polym. Chem. 44 (2006) 3751–3762.
[29] Y. Sutou, Y. Yin, Z. Hu, S. Chen, H. Kita, K. Okamoto, H. Wang, H. Kawasato, J. Polym. Sci. A: Polym. Chem. 47 (2009) 1463–1477.
[30] Z. Hu, Y. Yin, K. Yaguchi, N. Endo, M. Higa, K. Okamoto, Polymer 50 (2009) 2933–2943.
[31] H. Bi, S. Chen, X. Chen, K. Chen, N. Endo, M. Higa, K. Okamoto, L. Wang, Macromol. Rapid Commun. 30 (2009) 1852–1856.
[32] N. Endo, K. Matsuda, K. Yaguchi, Z. Hu, K. Chen, M. Higa, K. Okamoto, J. Electrochem. Soc. 156 (2009) B628–B633.
[33] K. Yaguchi, K. Chen, N. Endo, M. Higa, K. Okamoto, J. Power Sources 195 (2010) 4676–4684.
[34] K. Okamoto, K. Yaguchi, H. Yamamoto, K. Chen, N. Endo, M. Higa, H. Kita, J. Power Sources 195 (2010) 5856–5861.
[35] N. Asano, M. Aoki, S. Suzuki, K. Miyatake, H. Uchida, M. Watanabe, J. Am. Chem. Soc. 128 (2006) 1762–1770.
[36] A. Kabasawa, J. Saito, H. Yano, K. Miyatake, H. Uchida, M. Watanabe, Electrochim. Acta 54 (2009) 1076–1082.
[37] Z. Qiu, S. Wu, Z. Li, S. Zhang, W. Xing, C. Liu, Macromolecules 39 (2006) 6425–6432.
[38] C.H. Lee, C.H. Park, Y.M. Lee, J. Membr. Sci. 313 (2008) 199–206.
[39] S.D. Mikhailenko, G.P. Robertson, M.D. Guiver, S. Kaliaguine, J. Membr. Sci. 285 (2006) 306–316.
[40] C. Zhang, X. Guo, J. Fang, H. Xu, M. Yuan, B. Chen, J. Power Sources 170 (2007) 42–45.
[41] S. Zhong, X. Cui, H. Cai, T. Fu, C. Zhao, H. Na, J. Power Sources 164 (2007) 65–72.
[42] X. Chen, P. Chen, Z. An, K. Chen, K. Okamoto, J. Power Sources 196 (2011) 1694–1703.
[43] M. Kido, Z. Hu, T. Ogo, Y. Sutou, K. Okamoto, J. Fang, Chem. Lett. 36 (2007) 272–273.
[44] J. Fang, F. Zhai, X. Guo, H. Xu, K. Okamoto, J. Mater. Chem. 17 (2007) 1102–1108.
[45] X. Cheng, J. Zhang, Y. Tang, C. Song, J. Shen, D. Song, J. Zhang, J. Power Sources 167 (2007) 25–31.
[46] Y. Song, J.M. Fenton, H.R. Kunz, L.J. Bonville, M.V. Williams, J. Electrochem. Soc. 152 (2005) A539–A544.
[47] M. Inaba, T. Kinumoto, M. Kiriaki, R. Umebayashi, A. Tasaka, Z. Ogumi, Electrochim. Acta 51 (2008) 5746–5753.